Journal of Materials Chemistry C

ROYAL SOCIETY OF CHEMISTRY

PAPER

View Article Online
View Journal | View Issue

Cite this: J. Mater. Chem. C, 2022, 10, 2663

Crystalline organic thin films for crystalline OLEDs (I): orientation of phenanthroimidazole derivatives†

Dan Liu, [ab] Feng Zhu *[ab] and Donghang Yan[ab]

Received 9th September 2021,
Accepted 28th December 2021

DOI: 10.1039/d1tc04286f

rsc.li/materials-c

Compared with traditional organic light-emitting diodes (OLEDs) based on amorphous thin films, crystalline OLEDs possess promising advantages in developing advanced display technologies, such as a longer lifetime and a lower driving voltage. In recently developed crystalline OLEDs, the crystalline thin films of 2-(4-(9*H*-carbazol-9-yl)phenyl)-1-(3,5-difluorophenyl)-1*H*-phenanthro [9,10-*d*]imidazole (2FPPICz) grown *via* the weak epitaxy growth (WEG) method determined the device performance and played a crucial role in achieving a superior photon output capability. However, the structural properties of such novel crystalline thin films remain to be investigated. Herein, we report the single-crystal structure of 2FPPICz and the WEG mechanism of the 2FPPICz crystalline thin film. The 2FPPICz molecules adopt an edge-on arrangement and the molecular long axis tends to be parallel to the inducing layer and substrate, indicating that the transition dipole moment is nearly horizontal. These unique orientation phenomena are attributed to the lattice matching that is established between the WEG and the inducing layers. This work on the 2FPPICz crystalline thin film provides a structural foundation for the further development of crystalline OLEDs.

Introduction

Crystalline thin films of organic semiconductors with high molecular orientation and high thermal stability have attracted extensive attention over the years.[1–4] Distinguished from amorphous organic thin films, crystalline thin films are expected to significantly improve the device performance in terms of the charge transport, light outcoupling efficiency and the device lifetime in organic light-emitting diodes (OLEDs).[5–7] However, high-performance OLEDs based on the crystalline route have not been widely realized even after many efforts. Recently, it was reported that efficient deep-blue luminescence has been achieved in crystalline OLEDs that consist of phenanthroimidazole derivatives,[8,9] which were fabricated *via* a facile physical vapor deposition technique, the weak epitaxy growth (WEG) method.[10,11] Phenanthroimidazole derivatives are a class of promising deep-blue light-emitting materials due to their advantages of having a wide-bandgap, bi-polar transport and high fluorescence quantum yield.[12–17] A deep-blue fluorescent phenanthroimidazole derivative named 2-(4-(9*H*-carbazol-9-yl)phenyl)-1-(3,5-difluorophenyl)-1*H*-phenanthro [9,10-***d***]imidazole (2FPPICz) has been developed in which the introduction of *meta*-substituted fluorine atoms helps to regulate the properties of the excited-state, so as to obtain the high blue emission performance.[15] Moreover, the reported doped crystalline thin-film OLED (C-OLED) that adopted 2FPPICz as the host material has demonstrated an excellent performance with the largest number of emitted photons in deep-blue OLEDs compared with all reported amorphous thin-film deep-blue OLEDs.[9] These promising properties are ascribed to the 2FPPICz crystalline thin films, which render a high mobility for superior charge transport and rapid exciton formation. Therefore, the 2FPPICz crystalline thin film can act as an ideal matrix for improving the emitting performance of devices and developing next-generation OLEDs. However, the structure information of the 2FPPICz crystalline thin film is still ambiguous, which should be urgently tackled for the development of C-OLEDs.

In this work, we report the detailed structure of the 2FPPICz crystal and the fundamental growth mechanism of the 2FPPICz WEG crystalline thin film on *p*-sexiphenyl (*p*-6P) layers. The crystalline structure of the thin films has been investigated using atomic force microscopy (AFM), X-ray diffraction (XRD), transmission electron microscopy (TEM) and selected area electron diffraction (SAED). 2FPPICz molecules are inclined to be horizontally oriented on *p*-6P films, which is different from previously reported WEG thin films. In addition, there is only

[a] State Key Laboratory of Polymer Physics and Chemistry, Changchun Institute of Applied Chemistry, Chinese Academy of Sciences, Changchun 130022, China. E-mail: zhufeng@ciac.ac.cn

[b] School of Applied Chemistry and Engineering, University of Science and Technology of China, Hefei 230026, China

† Electronic supplementary information (ESI) available. CCDC 2106623. For ESI and crystallographic data in CIF or other electronic format see DOI: 10.1039/d1tc04286f

one orientation of 2FPPICz molecules on the *p*-6P double-layer domains. The oriented nucleation and growth of the 2FPPICz film are related to the surface geometrical channels of the *p*-6P substrate. The high orientation of crystalline thin films provides the prerequisite for excellent charge transport and photon output in the out-of-plane direction, which are critical for obtaining high-performance C-OLEDs.

Results and discussion

The synthesis and characterization of the 2FPPICz material has been described in a previous study,[15] but the crystalline structure information has not yet been elucidated. In order to acquire the molecular packing modes of 2FPPICz (the molecular structure as shown in Fig. 1a), single crystals were grown *via* solvent diffusion in which dichloromethane and methanol were the good solvent and the poor solvent, respectively (Fig. S1, ESI†). Crystals with a columnar shape were obtained, as shown in Fig. 1b. The molecular packing mode of the 2FPPICz single crystal and the unit cell dimensions are exhibited in Fig. 1c. The crystallographic data reveal that there are four molecules ($Z = 4$) in the unit cell with the structural motif containing two molecules ($Z' = 2$, the two molecules on the left). Fig. 1d gives the dihedral angles of the two molecules in the structural motif. One of the molecules adopts a twisted conformation with torsion angles of 78.3° between the phenyl-phenanthroimidazole (PPI) groups and the N-bounded phenyl rings, 39.2° between the PPI groups and the central benzene rings, as well as 43.2° between the central benzene rings and the carbazole (Cz) groups, while the other adopts the angles of 77.7°, 37.7° and 43.4° in turn. These distinctions are related to the intermolecular interaction forces as shown in Fig. 1e. In each of the structural motifs, C–H···N hydrogen bonds form between the hydrogen of N-bounded phenyl rings and the adjacent molecule nitrogen of the PPI moieties at a distance of 2.737 Å, and C–H···F hydrogen bonds between the hydrogen of the PPI moieties and the adjacent molecule fluorine are formed at a distance of 2.640 Å, as well as n–π interactions assembling between the lone pair electrons on the fluorine and PPI moieties. In addition, there are also C–H···π interactions linked in a herringbone structure at different distances of 3.173 Å, 2.712 Å, 2.730 Å and 3.141 Å, respectively. The packing modes are fundamental for studying the crystalline thin-film structure. Moreover, the relatively large crystal density (Table S2 (ESI†), ρ column) reveals that 2FPPICz molecules pile up in a more compact form on account of the fluorine substitution compared with other reported PPI derivatives,[18–20] which is substantially beneficial to decrease the non-radiative decay caused by molecular vibration.[21] Measurement of ^{19}F NMR spectra characterizes the fluorinated fluorophore as shown in Fig. S2 (ESI†). In addition, the polar space group is very rare in pure organic molecules, which may bring new properties in future applications.

The WEG method provides an effective and facile way to prepare high-quality crystalline organic films, which can induce the nucleation and growth of subsequent layers by introducing highly ordered rod-like molecular layers.[10,11] The growth of large-area continuous organic thin films with high orientation and low defects is deterministic for obtaining high-performance devices. Fig. 2a displays the molecular structure of *p*-6P, a rod-like molecule that is frequently used as the inducing layer and which is crucial for the WEG growth of the active layers. Different thickness films of *p*-6P deposited on Si/SiO_2 revealed that the thin films consisted of large-size domains (Fig. S3, ESI†). As the coverage increases, the domains fuse to form a continuous thin film with a molecularly smooth surface of which the root-mean square (RMS) roughness is less than 2 nm. After condition optimization, the 2FPPICz molecules were deposited on double-layer films of *p*-6P (Fig. 2b). 2FPPICz thin films with different thicknesses were prepared. As illustrated in Fig. 2c, 2FPPICz islands with a dominant growth direction were formed on the *p*-6P double-layer. The islands became larger and met with their neighbours as the thickness increased (Fig. 2d). Subsequently, the crystal domains merged with the ones around them until the whole *p*-6P layer was covered. A stripe-like continuous crystalline thin film was achieved in the end (Fig. 2e). The size of the domains was similar to that of *p*-6P and the crystalline strips exhibited an obvious in-plane orientation in each *p*-6P domain, demonstrating that a well-defined epitaxial form between *p*-6P and the 2FPPICz thin films was established. Fig. 2f shows the morphology of 20 nm-thick 2FPPICz thin film with an RMS surface roughness of less than 3 nm. These smooth and highly ordered 2FPPICz thin films are the basis of fabricating high-performance devices.

For insight into the structural characteristics of the crystalline thin films, X-ray diffraction (XRD) measurements were carried out. Fig. 3a depicts the out-of-plane XRD patterns of the thin films of double-layer *p*-6P and *p*-6P/2FPPICz (20 nm 2FPPICz on *p*-6P). The diffraction peak at $2\theta = 6.22°$ of the *p*-6P thin films (black solid line) corresponds to the (002) reflection in keeping with previous reports. As a result, the *p*-6P molecules stand upright on the substrate with a tilting angle of approximately 14°.[22] There are evident diffraction peaks in both the out-of-plane and in-plane XRD patterns of the WEG 2FPPICz thin-film (red solid line, Fig. 3a and b), demonstrating that the 2FPPICz molecules are arranged in an orderly fashion in the WEG films. Furthermore, the peaks around the primary peak ($2\theta = 9.14°$) in the out-of-plane XRD pattern, which are from the Laue oscillations, also prove the high crystallinity and good uniformity of the thin film.[23] The diffraction peak at $2\theta = 9.14°$ in the out-of-plane XRD pattern and at $2\theta = 20.68°$ in the in-plane XRD pattern can separately be assigned to the $(\bar{2}02)$ and (303) reflections according to the 2FPPICz single-crystal structure mentioned above.

Transmission electron microscopy (TEM) and selected area electron diffraction (SAED) experiments were carried out to study the epitaxial relationship between the 2FPPICz and *p*-6P thin films. Fig. S4 (ESI†) reveals the SAED pattern and the corresponding electron micrograph of the double-layer *p*-6P domains. The SAED pattern shows an orthogonal two-dimensional lattice consisting of the [001] zone, which is consistent with previous results.[22] A typical SAED pattern of 2FPPICz (20 nm) grown on the *p*-6P double-layer thin films was

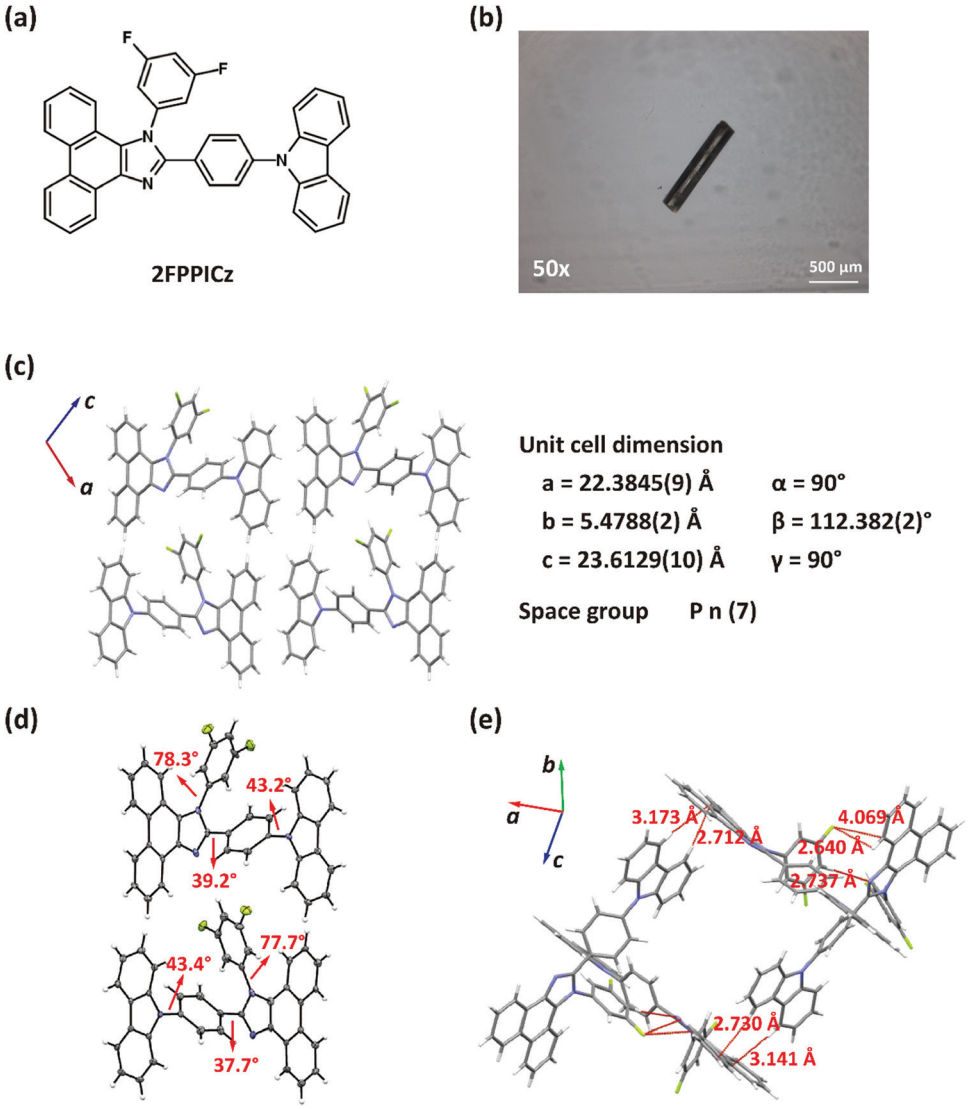

Fig. 1 (a) Molecular structure of 2FPPICz. (b) Optical micrograph of the 2FPPICz single crystal. (c) Molecular packing mode of the 2FPPICz single crystal and the unit cell dimensions. (d and e) Oak Ridge thermal ellipsoid plots (ORTEPs) with the torsion angles marked (d) and the major intermolecular interactions (e) in the crystal of 2FPPICz.

observed, as illustrated in Fig. 4a. The indexed pattern shows that there was only one kind of in-plane orientation of the 2FPPICz molecules on the *p*-6P thin film. Moreover, the *b**-axis of the 2FPPICz crystal was parallel to the *b**-axis of the *p*-6P crystal. The epitaxial relationship between them was as follows: $(\bar{1}01)_{2FPPICz}//(001)_{p\text{-}6P}$, $[101]_{2FPPICz}//[100]_{p\text{-}6P}$, and $[010]_{2FPPICz}//[010]_{p\text{-}6P}$, which can be explained on the basis of two-dimensional lattice matching between the crystals of 2FPPICz and *p*-6P as described by the dashed grid in Fig. 4a. Along the direction of $[101]_{2FPPICz}$ and $[100]_{p\text{-}6P}$, the mismatching between the three-times interplane distance of 2FPPICz (yellow dashed-line box) and the five-times interplane distance of *p*-6P (red dashed-line box) is 2.39% (mismatching% = $(|3d(101)_{2FPPICz} - 5d(100)_{p\text{-}6P}|)/(5d(100)_{p\text{-}6P})$ = 2.39%). Along the direction of $[010]_{2FPPICz}$ and $[010]_{p\text{-}6P}$, the (010) diffraction point of 2FPPICz coincides with the (010) of *p*-6P and the mismatching between them is 0.18% (mismatching% = $(|d(010)_{2FPPICz} - d(010)_{p\text{-}6P}|)/(d(010)_{p\text{-}6P})$ = 0.18%). Their interplanar spacings are shown in Table S1 (ESI†) where the interplanar spacing of *p*-6P refers to previous reports and that of 2FPPICz is taken from the average values measured in the SAED patterns.[22] The mismatching is much smaller than the upper limit (10–15%) for the occurrence of organic epitaxy.[24] This almost perfect epitaxial relationship is important for preparing highly ordered crystalline WEG thin films in which the inducing layer acts in a deterministic role. Likewise, the morphology of the 2FPPICz WEG thin films is connected to the difference of the lattice mismatch between the $[010]_{2FPPICz}$ and $[101]_{2FPPICz}$ directions. As we can see, the [010] and [101] directions of 2FPPICz, respectively, correspond to the long-axis and short-axis directions of the stripe-like crystal comparing the SAED pattern with the electron micrograph (Fig. 4b). This is owing to the lattice mismatch that will accumulate along with the stacking of the unit cells. When a certain direction reaches the upper limit, the unit cells will not

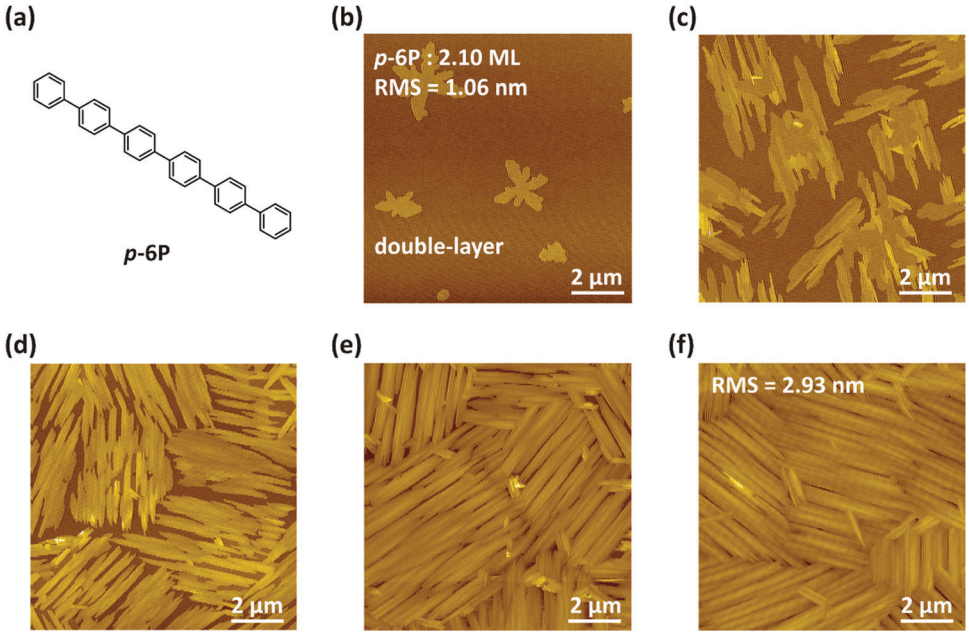

Fig. 2 (a) Molecular structure of *p*-6P. (b–f) AFM images of the 2.10 monolayer *p*-6P (b) and WEG crystalline films of 2FPPICz deposited on *p*-6P with different thicknesses of 1.5 nm (c), 5 nm (d), 10 nm (e), and 20 nm (f).

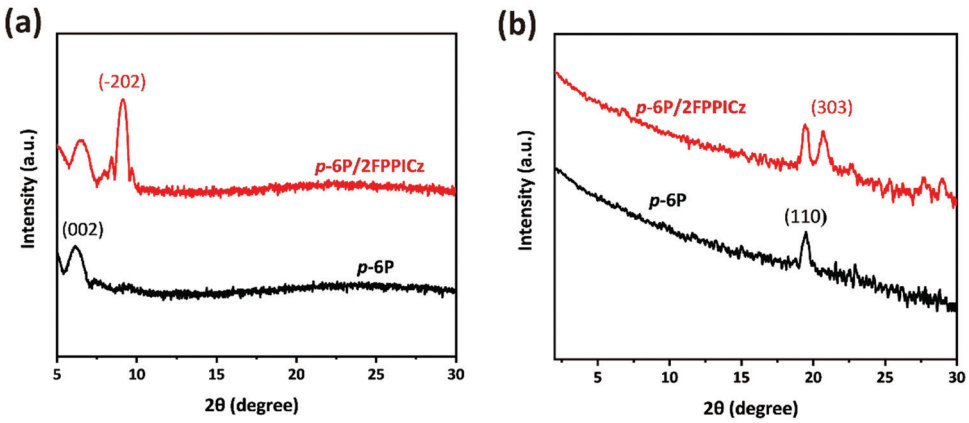

Fig. 3 (a) Out-of-plane and (b) in-plane XRD patterns of double-layer *p*-6P and 20 nm WEG 2FPPICz crystalline thin films.

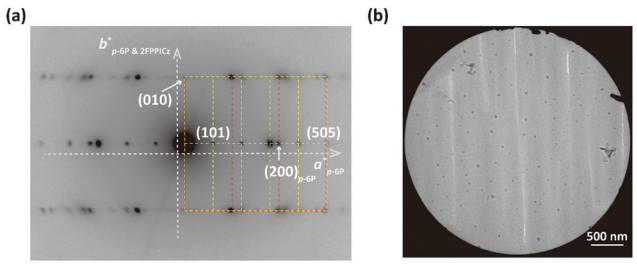

Fig. 4 SAED patterns (a) and the corresponding electron micrograph (b) of 2FPPICz thin films deposited on the *p*-6P double-layer. The red and yellow dashed grids represent the crystal lattices of *p*-6P and 2FPPICz, respectively.

be able to pile up in this direction. As a consequence, a larger number of unit cells are able to be stacked continuously along the [010] direction because of the smaller lattice mismatch compared with the [101] direction, which leads to the morphology of the thin films appearing as stripe-like crystals.

On the basis of a detailed analysis of the SAED patterns, the epitaxial mechanism of 2FPPICz deposited on the *p*-6P double-layer can be clarified. Along the [110] and [1$\bar{1}$0] directions of *p*-6P, there are geometrical channels formed by the prominent hydrogens on the surface as the black dashed arrow depicted in Fig. 5c. The 2FPPICz molecules have two kinds of conformation in the single crystal. The distance between the parallel molecules in the herringbone structure is 3.91 Å in one of the conformations and the other is 3.88 Å (Fig. 5b), which are both smaller than the distance of 4.57 Å for the [110] and [1$\bar{1}$0] channels (Fig. 5a). The wide enough channels enable each conformation of 2FPPICz molecules to set, which is effective

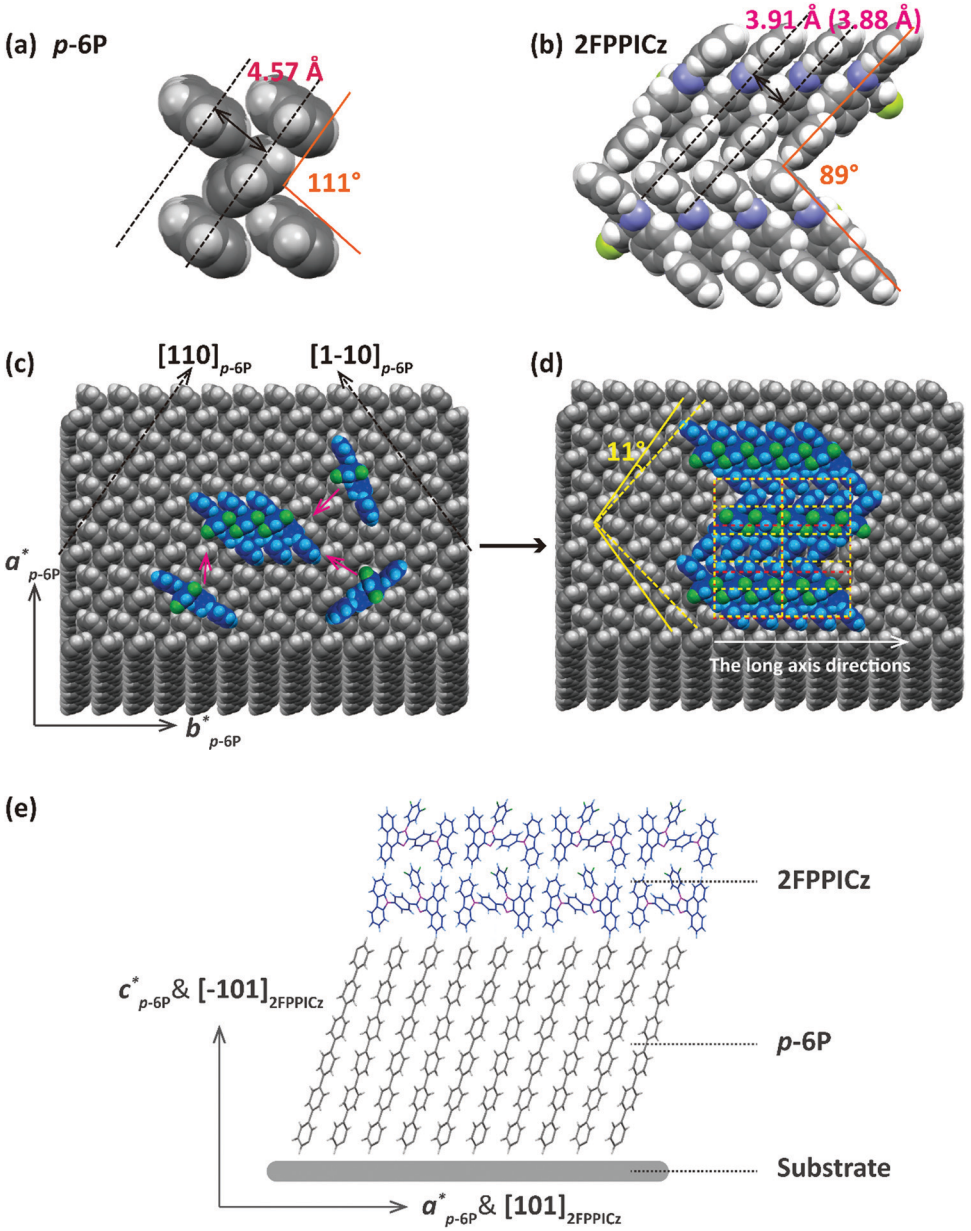

Fig. 5 (a and b) Crystal structures of *p*-6P and 2FPPICz as viewed along the *c* axis and the [$\bar{1}$01] projection, respectively. (c) Nucleation of 2FPPICz molecules in the channel of *p*-6P formed by prominent hydrogen atoms on the surface. (d) Schematic diagram of 2FPPICz deposited on the *p*-6P double-layer. The yellow solid lines and dashed lines represent the channel directions of *p*-6P and the long-axis directions of 2FPPICz, respectively. The red and yellow dashed grids, respectively, represent the crystal lattice of *p*-6P and 2FPPICz. (e) Packing modes of the 2FPPICz molecules on *p*-6P and the substrate.

for arranging the orientation of the 2FPPICz molecules. Since the [110] and [1$\bar{1}$0] channels are the same except for their directions, we take the nucleation of 2FPPICz molecules in one kind of channel as an example. First of all, some 2FPPICz molecules diffuse into the channels for the minimum potential energy because the surface channels are the best locations for the molecular break.[25,26] In the next moment, subsequent 2FPPICz molecules will nucleate with the preceding ones along the [110] channel to form the monomolecular columnar nucleus under van der Waals forces. With the growth of the crystal nucleus, a second molecular column begins to appear. It is not able to be arranged into the [1$\bar{1}$0] channel that is restricted by the herringbone structure with an angle of 89°, while the angle between the [110] and [1$\bar{1}$0] channels is 111°. The molecules will adjust to a more stable position determined by the lattice matching, which provides the lowest potential energy.[27] Therefore, the long axis of the 2FPPICz molecules, respectively, twists about 11° in the [110] and [1$\bar{1}$0] channels in the end. Because the angle of the herringbone structure of the two molecular conformations is the same, they can be

represented by the same epitaxial model as illustrated in Fig. 5d. The π–π stacking direction corresponds to the long-axis direction of the strip-like crystals and it is parallel to the substrate, contributing to improving charge mobility, which is important for obtaining a high photon output at low operating voltages.[28] The *p*-6P/2FPPICz thin-film transistors with gold source/drain electrodes were fabricated on Si/SiO_2 substrates to measure the carrier mobility, as shown in Fig. S5 (ESI†). The results demonstrated that the mobility of the crystalline films was significantly improved compared with that of the amorphous films, and was attributed to the highly ordered arrangement of molecules in the crystalline films. Combining the above tests and analysis, the packing modes of the 2FPPICz molecules on *p*-6P and the substrate can be established. The molecular long axes of 2FPPICz are nearly parallel to the substrate, as displayed in Fig. 5e, in contrast to the previously reported WEG thin films of, for example, metal phthalocyanines (MPcs), dinaphtho[2,3-b:2′,3′-*f*]thieno[3,2-*b*]thiophene (DNTT) and *N*,*N*′-diphenylperylene tetracarboxylic diimide (PTCDI–Ph) in which the molecules tend to be vertically oriented.[29–32] Besides, there are intermolecular interactions in the vertical direction (Fig. S6, ESI†). The carriers can transport in the vertical direction with a hole mobility of 0.10 $cm^2\ V^{-1}\ s^{-1}$ and an electron mobility of 0.015 $cm^2\ V^{-1}\ s^{-1}$, as measured in a previous study although the molecules adopt an edge-on arrangement on the substrate.[9] More importantly, the angle between the long axis and the substrate is 6.1° and the PPI moieties are perpendicular to the substrate. The electronic structures of 2FPPICz were calculated using density functional theory (DFT) in a previous study,[15] and the transition dipole moment was further calculated. The direction of the transition dipole moment possesses an angle of about 6.5° with the molecular long axes (Fig. S7, ESI†). Therefore, the direction of the transition dipole moment with a tiny angle of 0.4° with the substrate is nearly parallel, which is an advantage for improving the light-outcoupling efficiency because the radiation direction is perpendicular to the transition dipole moment.[33,34]

Conclusions

In summary, 2FPPICz, a novel wide-bandgap deep-blue light-emitting semiconductor material with bi-polar transport, can act as a host matrix for the construction of a novel class of crystalline OLEDs in which the 2FPPICz WEG crystalline thin film contributes greatly to the high performance. Thus, the structure information and growth behavior of the 2FPPICz crystalline thin films become key issues. In this paper, we have grown a single crystal of 2FPPICz to obtain the molecular packing modes as a foundation of the thin-film structure analysis and studied the morphology of the 2FPPICz crystalline thin-film grown epitaxially on the *p*-6P double-layer. Crystal analyses indicate that the molecules have a more compact stacking than other phenanthroimidazole derivatives and they possess polar space groups that are infrequent in pure organic molecules, which may bring more novel characteristics. In addition, characterization of the crystalline thin films demonstrated that the WEG thin films are highly oriented and possess good crystallinity. More importantly, the 2FPPICz molecules adopt an edge-on arrangement on the substrate and the long axis is almost parallel to the substrate, which is beneficial for improving the carrier mobility and light-outcoupling efficiency. This form is evidently different from the previously reported WEG molecular growth behavior. The formation of highly ordered WEG 2FPPICz thin films is related to the lattice matching between the inducing layer and the epitaxial layer. These results provide a structural foundation for the development of crystalline OLEDs.

Experimental section

Materials

p-Sexiphenyl (*p*-6P) was purchased from Jilin Oled Material Tech Co., Ltd 2-(4-(9*H*-Carbazol-9-yl) phenyl)-1-(3,5-difluorophenyl)-1*H*-phenanthro[9,10-*d*]imidazole (2FPPICz) was synthesized according to the previous report.[15] Both of them were purified twice *via* thermal gradient vacuum sublimation before use.

Single-crystal structure

The optical micrograph of the 2FPPICz single crystal was acquired using an optical microscope (OLYMPUS BX51, Japan). X-ray diffraction data for 2FPPIPCz were obtained employing the ω-scan mode with Mo Kα radiation (λ = 0.71073 Å) at the temperature of −173.15 °C using a Bruker APEX-II instrument at Jilin University. A dual-space algorithm using SHELXT and full-matrix least-squares calculations against F^2 using SHELXL were, respectively, used to solve and refine the structure;[35,36] these processes took place using Olex2 software.[37] CCDC† 2106623.

Fabrication and characterization of films

Before use, the Si/SiO_2 substrate was wiped with absorbent cotton soaked in acetone and then rinsed with acetone, ethanol, and deionized water in turn. This process was repeated three times and the substrate was desiccated using high-purity nitrogen in the end. After that, the Si/SiO_2 substrate was placed in a vacuum chamber at a pressure of under 10^{-4} Pa. The *p*-6P film was deposited on the Si/SiO_2 substrate using an evaporation rate of 2–3 Å min^{-1} at the substrate temperature of 160 °C. Subsequently, the 2FPPICz film was grown on the *p*-6P film at an evaporation rate of 2–4 Å min^{-1} at the lower substrate temperature of 110 °C. The evaporation rate and the thickness were monitored using a quartz-crystal microbalance. The morphologies of films were studied using an SPI 3800/SPA 300 HV (Seiko Instruments Inc., Japan) atomic force microscope (AFM) with tapping mode. The out-of-plane X-ray diffraction (XRD) data were collected using the locked coupled mode with Cu Kα radiation (λ = 1.54056 Å) of a thin-film diffractometer (Bruker D8 Discover). The in-plane XRD patterns were acquired using a Rigaku SmartLab X-ray diffraction instrument with Cu Kα radiation (λ = 1.54056 Å).

Selected area electron diffraction

Preparation and measurement of samples. Vacuum deposition of a carbon film on the surface of the thin films deposited

on the SiO_2/Si substrate as a supporting layer was carried out using an ETD-800C type small thermal evaporation coating instrument (Vision Precision Instruments Inc., China). Because of the different hydrophobicity and expansion coefficient between silica and the sample, the carbon film-fixed sample was transferred to the surface of a 10% hydrofluoric acid aqueous solution in a watch glass. Then the sample was captured using a 400 mesh copper grid, which was placed on filter paper to absorb water and dry it. The selected area electron diffraction patterns were obtained using a transmission electron microscope (JEOL JEM-1011) at an electron beam accelerating voltage of 100 kV, and the corresponding electron micrograph was acquired under bright field conditions.

Calibration of selected area electron diffraction pattern. The basic formula of electron diffraction in transmission electron microscopy is $Rd = \lambda L$, where R is the distance from the transmission spot to the diffraction spot, d is the interplanar spacing, λ is the electron wavelength, and L is the effective camera length. However, the camera length will change slightly as conditions change during the experiment. Therefore, the internal standard method was used for the accuracy of the experiment. Since L and λ of the standard sample and the tested sample are the same, the formula can be simplified as $R_{\text{sample}}d_{\text{sample}} = R_{\text{standard}}d_{\text{standard}}$. Hence, through measuring the distance from the transmission spot to the diffraction spot of the standard and tested samples, the interplanar spacing corresponding to the diffraction point of the tested sample can be calculated, which can then be indexed. The metal gold is usually used as an internal standard for calibration. Nevertheless, since research on the structure and phase state of the induced layer *p*-6P has been studied thoroughly in previous work, the induction layer *p*-6P can be used directly as the internal standard to avoid the cumbersome preparation of gold samples.

Theoretical calculations

The Gaussian 09 program was used for the theoretical calculations. The transition dipole moments were calculated using density functional theory (DFT) and time-dependent DFT (TD-DFT), which, respectively, optimize the ground- and excited-state configuration of the molecule through the B3LYP density functional method at the 6-31G (d) basis set.

Author contributions

F. Z. and D. H. Y. initiated and designed the research. D. L. carried out the growth and characterization of crystalline thin films. All authors discussed the results, analyzed the data and prepared the manuscript. F. Z. and D. H. Y. supervised the project.

Conflicts of interest

There are no conflicts to declare.

Acknowledgements

The authors thank: Prof. Yue Wang's research group at Jilin University for help in testing the single crystal; Dr J. C. Rao for DFT calculations; Prof. Jidong Zhang for analyzing structure data; Jilin Yuanhe Electronic Material Co. for support on preparing the materials. This work was supported by the National Key R&D Program of China (2017YFA0204704). This work is dedicated to the celebration for Prof. Daoben Zhu's 80th birthday.

Notes and references

1 Z. N. Bao, A. J. Lovinger and A. Dodabalapur, *Appl. Phys. Lett.*, 1996, **69**, 3066–3068.
2 R. J. Li, W. P. Hu, Y. Q. Liu and D. B. Zhu, *Acc. Chem. Res.*, 2010, **43**, 529–540.
3 J. L. Yang, D. H. Yan and T. S. Jones, *Chem. Rev.*, 2015, **115**, 422–500.
4 C. L. Wang, H. L. Dong, L. Jiang and W. P. Hu, *Chem. Soc. Rev.*, 2018, **47**, 5570–5603.
5 K. H. Kim, J. L. Liao, S. W. Lee, B. Sim, C. K. Moon, G. H. Lee, H. J. Kim, Y. Chi and J. J. Kim, *Adv. Mater.*, 2016, **28**, 2526–2532.
6 X. T. Zhang, H. L. Dong and W. P. Hu, *Adv. Mater.*, 2018, **30**, 1801048.
7 R. Ding, M. H. An, J. Feng and H. B. Sun, *Laser Photonics Rev.*, 2019, **13**, 1900009.
8 L. Liu, C. L. Li, Z. Q. Li, P. F. Sun, F. Zhu, Y. Wang and D. H. Yan, *Org. Electron.*, 2020, **84**, 105806.
9 J. H. Xin, P. F. Sun, F. Zhu, Y. Wang and D. H. Yan, *J. Mater. Chem. C*, 2021, **9**, 2236–2242.
10 H. B. Wang, F. Zhu, J. L. Yang, Y. H. Geng and D. H. Yan, *Adv. Mater.*, 2007, **19**, 2168–2171.
11 J. L. Yang and D. H. Yan, *Chem. Soc. Rev.*, 2009, **38**, 2634–2645.
12 J. Tagare and S. Vaidyanathan, *J. Mater. Chem. C*, 2018, **6**, 10138–10173.
13 Y. W. Xu, X. M. Liang, Y. Q. Liang, X. M. Guo, M. Hanif, J. D. Zhou, X. H. Zhou, C. Wang, J. W. Yao, R. Y. Zhao, D. H. Hu, X. F. Qiao, D. G. Ma and Y. G. Ma, *ACS Appl. Mater. Interfaces*, 2019, **11**, 31139–31146.
14 H. Zhang, B. Zhang, Y. W. Zhang, Z. Xu, H. Z. Wu, P. A. Yin, Z. M. Wang, Z. J. Zhao, D. G. Ma and B. Z. Tang, *Adv. Funct. Mater.*, 2020, **30**, 2002323.
15 J. H. Xin, Z. Q. Li, Y. J. Liu, D. Liu, F. Zhu, Y. Wang and D. H. Yan, *J. Mater. Chem. C*, 2020, **8**, 10185–10190.
16 J. Tagare, R. Boddula, S. S. Sudheendran, D. K. Dubey, J. H. Jou, S. Patel and S. Vaidyanathan, *J. Mater. Chem. C*, 2020, **8**, 16834–16844.
17 J. Tagare, R. A. K. Yadav, S. S. Swayamprabha, D. K. Dubey, J. H. Jou and S. Vaidyanathan, *J. Mater. Chem. C*, 2021, **9**, 4935–4947.
18 Y. Zhang, S. L. Lai, Q. X. Tong, M. F. Lo, T. W. Ng, M. Y. Chan, Z. C. Wen, J. He, K. S. Jeff, X. L. Tang,

W. M. Liu, C. C. Ko, P. F. Wang and C. S. Lee, *Chem. Mater.*, 2011, **24**, 61–70.
19 Y. Tan, Z. F. Zhao, L. Shang, Y. Liu, C. Wei, J. Y. Li, H. B. Wei, Z. W. Liu, Z. Q. Bian and C. H. Huang, *J. Mater. Chem. C*, 2017, **5**, 11901–11909.
20 Z. Q. Li, N. Xie, Y. C. Xu, C. L. Li, X. Y. Mu and Y. Wang, *Org. Mater.*, 2020, **2**, 11–19.
21 M. P. Li, K. Ling, H. F. Shi, N. Gan, L. L. Song, S. Z. Cai, Z. C. Cheng, L. Gu, X. Wang, C. Q. Ma, M. X. Gu, Q. Wu, L. F. Bian, M. L. Liu, Z. F. An, H. L. Ma and W. Huang, *Adv. Opt. Mater.*, 2019, **7**, 1800820.
22 J. L. Yang, T. Wang, H. B. Wang, F. Zhu, G. Li and D. H. Yan, *J. Phys. Chem. B*, 2008, **112**, 3132–3137.
23 A. C. Dürr, F. Schreiber, M. Münch, N. Karl, B. Krause, V. Kruppa and H. Dosch, *Appl. Phys. Lett.*, 2002, **81**, 2276–2278.
24 J. C. Wittmann and B. Lotz, *Prog. Polym. Sci.*, 1990, **15**, 909–948.
25 M. Campione, A. Sassella, M. Moret, A. Papagni, S. Trabattoni, R. Resel, O. Lengyel, V. Marcon and G. Raos, *J. Am. Chem. Soc.*, 2006, **128**, 13378–13387.
26 V. Marcon, G. Raos, M. Campione and A. Sassella, *Cryst. Growth Des.*, 2006, **6**, 1826–1832.
27 S. R. Forrest, *Chem. Rev.*, 1997, **97**, 1793–1896.
28 M. Pope and C. Swenberg, *Electronic Processes In Organic Crystals*, Oxford University Press, 1999.
29 H. B. Wang, D. Song, J. L. Yang, B. Yu, Y. H. Geng and D. H. Yan, *Appl. Phys. Lett.*, 2007, **90**, 253510.
30 T. Wang, J. L. Yang, H. B. Wang, F. Zhu and D. H. Yan, *J. Phys. Chem. B*, 2008, **112**, 6786–6792.
31 L. Z. Huang, F. Zhu, C. F. Liu, H. B. Wang, Y. H. Geng and D. H. Yan, *Org. Electron.*, 2010, **11**, 195–201.
32 H. Chang, Y. F. Deng, Y. H. Geng, T. Wang and D. H. Yan, *Org. Electron.*, 2015, **22**, 86–91.
33 D. Yokoyama, *J. Mater. Chem.*, 2011, **21**, 19187–19202.
34 T. D. Schmidt, T. Lampe, D. Sylvinson, M. R. Peter, I. Djurovich, M. E. Thompson and W. Brütting, *Phys. Rev. Appl.*, 2017, **8**, 037001.
35 G. M. Sheldrick, *Acta Crystallogr., Sect. C: Struct. Chem.*, 2015, **71**, 3–8.
36 G. M. Sheldrick, *Acta Crystallogr., Sect. A: Found. Adv.*, 2015, **71**, 3–8.
37 O. V. Dolomanov, L. J. Bourhis, R. J. Gildea, J. A. K. Howard and H. Puschmann, *J. Appl. Crystallogr.*, 2009, **42**, 339–341.

